

Measurement of two-qubit states by quantum point contacts

Tetsufumi Tanamoto¹ and Xuedong Hu²

¹Corporate R&D Center, Toshiba Corporation, Saiwai-ku, Kawasaki 212-8582, Japan,

²Department of Physics, University at Buffalo, SUNY, Buffalo, New York 14260-1500, USA

We solve the master equations of two charged qubits measured by two serially coupled quantum point contacts (QPCs). We describe two-qubit dynamics by comparing entangled states with product states, and show that the QPC current can be used for reading out results of quantum calculations and providing evidences of two-qubit entanglement. We also calculate the concurrence of the two qubits as a function of dephasing rate that originates from the measurement. We conclude that coupled charge qubits can be effectively detected by a QPC-based detector.

I. INTRODUCTION

Quantum information processing in charge-based solid state nanostructures has attracted wide spread attention because of the potential scalability of such devices, and the relative ease with which such charge devices can be manipulated and detected.^{1,2,3,4} Recently, two-qubit coherent evolution and possibly entanglement have been observed in capacitively coupled Cooper pair boxes.⁵ For universal quantum computing, two-qubit operations are required, so that the realization of controlled two-qubit entanglement is regarded as a crucial milestone for the study of solid state quantum computing. While two-qubit information can be detected with one measurement device on each qubit, it is also important to search for a detector that is directly sensitive to two-qubit information, and to develop a proper formalism to study two-qubit measurement processes.^{6,7,8}

The ultimate criterion for the detection of qubits is whether we can distinguish the results of a quantum computation by the output signal of the detector, *e.g.* current or conductance of a single electron transistor. In the case of one qubit, two single-qubit states $|\downarrow\rangle$ and $|\uparrow\rangle$ need to be distinguished. In the case of two qubits, four two-qubit state, $|\downarrow\downarrow\rangle$, $|\downarrow\uparrow\rangle$, $|\uparrow\downarrow\rangle$, and $|\uparrow\uparrow\rangle$ (we will call them $|A\rangle \sim |D\rangle$) need to be distinguished before the qubit states are destroyed by the measurement. As we mentioned above, measurement of multi-qubit states can generally be achieved by multiple single-qubit measurements on each of the qubits, respectively. Here we study a different detection process: the temporal behavior of a detector (QPC in the present study) that simultaneously couples to two qubits. We show that information contained in the temporal evolution of the QPC current can help us distinguish different two-qubit product states, and some entangled states from the product states. Indeed, one motivation of our study is to obtain direct evidence for the entanglement of the qubits, possibly from the detector current or other measurable quantities.

In Ref. 8, we studied a particular scheme for the quantum measurement of two charge qubits by a two-island single-electron transistor (SET), and showed that the SET is an effective detector of the two-charge-qubit states. Here the charge qubits are constituted of two coupled quantum dots (QD) with one excess electron. Due

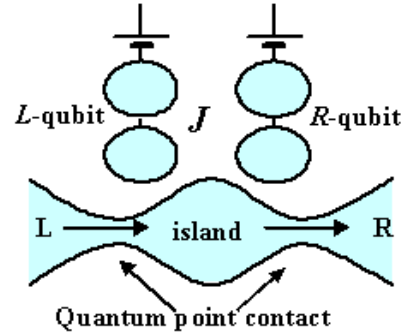


FIG. 1: Two charge qubits (using double quantum dot charged states) are capacitively coupled to a detector of two serially coupled QPCs. J is the strength of inter-qubit interaction. No tunneling is allowed between the QPC detector and any of the qubits.

to tunnel coupling of the QDs, the wave functions in a qubit are superpositions of localized states from each of the QDs. If a qubit is prepared in a single QD state, it tends to oscillate between the two sides of the double QD. If we define the local states as $|\uparrow\rangle$ and $|\downarrow\rangle$, the qubit state oscillates between the two logical states with a frequency determined by the tunneling coupling and the difference of the energy-levels of the two QDs. Time-dependent behavior of this coherent oscillation of the qubits is determined by the initial state. If we take the initial time to be that when a final quantum operation is applied to the qubit, the detector readout current reflects the results of quantum calculation. The qubit states interact with the readout current by changing the energy (and therefore occupation) of the electronic states in the SET islands and possibly the tunneling rates of the junctions (by modifying the island electronic states themselves) on both sides of the islands. Although, in Ref. 8, we show that the SET can distinguish the different coherent oscillations between the two-qubit product states and the entangled states, we have not yet investigated the two-qubit dynamics itself.

Here we would like to study quantum point contact (QPC) as a detector for two coupled charge qubits (Fig. 1). A QPC is essentially a one-dimensional conducting channel and is considered to be an effective charge de-

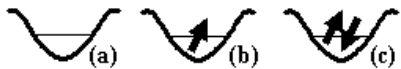


FIG. 2: Electronic states in the inter-QPC island. We assume that there is only one accessible electronic orbital state on the island. There are thus totally four possible island states: (a) Empty dot—state "a" has no excess electron on the dot. (b) Single-electron dot—state "b" has one electron and is spin-degenerate. (c) Two-electron dot—state "c" has two electrons in a spin singlet state occupying the same orbital state.

tector, similar to the SET. The particular scheme we consider consists of two low transparency QPCs connected in series through a single level quantum dot. Each of the QPCs is close to a charge qubit so that its current/conductance is dependent on the state of the respective qubit. Compared to the SET detector, the QPC detector interacts with qubits only through the change of tunneling rates. Although the SET detector is able to describe a variety of features of the internal states of qubits in Ref.⁸, we could not identify which of the two interactions (that between the islands and qubits, which modify the level occupations on the SET islands; or that between the tunneling junctions and qubits, where potential by the qubits modifies the tunneling rates) plays the major role in the SET detector. Thus, an important question is whether or not the QPC detector that interacts with qubits only by the change of the tunneling rates is also an effective apparatus for detecting the qubit states. In this paper, after discussing the basic two-qubit dynamics with no detector, we focus mainly on the following issues: (1) whether we can distinguish the four product states $|A\rangle \sim |D\rangle$ of two coupled charge qubits in the time-domain with a serially coupled QPC detector, (2) whether we can distinguish the entangled states from the product states of these two qubits, and (3) whether the quantum Zeno effects in the coupled charge qubits can be observed. In the following sections, we solve the master equations for the coupled qubit-QPC system and investigate the effectiveness of the proposed QPC detector. In Sec. II, we present our formulation of two qubits and the QPC detector. In Sec. III, we discuss the difference between a dynamics of single qubit and that of two qubits. In Sec. IV, we show the numerical results of two-qubit detection by QPC. Sec. V is devoted to discussion for the QPC detection, and Sec. VI consists of a conclusion.

II. FORMULATION

In the present measurement scheme, the QPCs are capacitively coupled to the charge qubits (Fig. 1), so that the current through them sensitively depends on the states of the qubits. We describe the two QPCs using two tunnel matrix elements only and neglect further

internal structures.^{9,10} We assume that the qubit-QPC coupling is purely capacitive, so that there is no current flowing from the qubits to either of the QPC electrodes. The Hamiltonian for the combined two qubits and the QPCs is written as $H = H_{\text{qb}} + H_{\text{qpc}} + H_{\text{int}}$. H_{qb} describes the two interacting qubits (left and right, as illustrated in Fig. 1), each consisting of two tunnel-coupled QDs and one excess charge:⁶

$$H_{\text{qb}} = \sum_{\alpha=L,R} (\Omega_{\alpha}\sigma_{\alpha x} + \Delta_{\alpha}\sigma_{\alpha z}) + J\sigma_{Lz}\sigma_{Rz}, \quad (1)$$

where Ω_{α} and Δ_{α} are the inter-QD tunnel coupling and energy difference (gate bias) within each qubit. Here we use the spin notation such that $\sigma_{\alpha x} \equiv a_{\alpha}^{\dagger}b_{\alpha} + b_{\alpha}^{\dagger}a_{\alpha}$ and $\sigma_{\alpha z} \equiv a_{\alpha}^{\dagger}a_{\alpha} - b_{\alpha}^{\dagger}b_{\alpha}$ ($\alpha = L, R$), where a_{α} and b_{α} are the annihilation operators of an electron in the upper and lower QDs of each qubit. Thus, $|\uparrow\rangle$ and $|\downarrow\rangle$ refer to the two single-qubit states in which the excess charge is localized in the upper and lower dot, respectively. J is a coupling constant between the two qubits, originating from capacitive couplings in the QD system.⁶

The two serially coupled QPCs are described by H_{qpc} :

$$H_{\text{qpc}} = \sum_{\substack{\alpha=L,R \\ s=\uparrow,\downarrow}} \sum_{i_{\alpha}} \left[E_{i_{\alpha}} c_{i_{\alpha}s}^{\dagger} c_{i_{\alpha}s} + V_{i_{\alpha}s} (c_{i_{\alpha}s}^{\dagger} d_s + d_s^{\dagger} c_{i_{\alpha}s}) \right] + \sum_{s=\uparrow,\downarrow} E_d d_s^{\dagger} d_s + U d_{\uparrow}^{\dagger} d_{\uparrow} d_{\downarrow}^{\dagger} d_{\downarrow}. \quad (2)$$

Here $c_{i_{L}s}(c_{i_{R}s})$ is the annihilation operator of an electron in the i_{L} th (i_{R} th) level ($i_{L}(i_{R}) = 1, \dots, n$) of the left (right) electrode, d_s is the electron annihilation operator of the island between the QPCs, $E_{i_{L}s}(E_{i_{R}s})$ is the energy level of electrons in the left (right) electrode, and E_d is that of the island. Here we assume only one energy level on the island between the two QPCs, with spin degeneracy. $V_{i_{L}s}(V_{i_{R}s})$ is the tunneling strength of electrons between the left (right) electrode state $i_{L}s$ ($i_{R}s$) and the island state. U is the on-site Coulomb energy of double occupancy in the island. Note that the number of island states here (Fig. 2) is much smaller than that of the two-island SET states,⁸ where we need to take into account at least 10 types of detector states. In Ref. 8, we observed that the two-island SET can represent a variety of qubit states because of its large number of degrees of freedom. With a much simpler state structure for the present coupled QPC scheme, we will study whether the QPC current could still represent the qubit states with sufficient clarity.

The capacitive interaction between the qubits and the QPCs is represented by H_{int} , which contains the information that localized charge near the QPCs increases the energy of the system electrostatically, thus affecting the tunnel coupling between the QPCs and the island in between:⁹

$$H_{\text{int}} = \sum_{\alpha=L,R} \sum_{i_{\alpha},s} \delta V_{i_{\alpha}s} (c_{i_{\alpha}s}^{\dagger} d_s + d_s^{\dagger} c_{i_{\alpha}s}) \sigma_{\alpha z}, \quad (3)$$

where $\delta V_{i_\alpha s}$ is an effective change of the tunneling strength between the electrodes and QPC island (we shift the origin of the interaction energy such that $\delta V_{i_\alpha s} = 0$ corresponds to the case where qubits are not polarized $\sigma_{\alpha z} = 0$). We assume that the tunneling strength of electrons weakly depends on the energy $V_{i_\alpha s} = V_\alpha(E_{i_\alpha s})$ and electrodes are degenerate up to the Fermi surface. Then the qubit-QPC interaction dictates that qubit states influence the QPC tunneling rate in the form of $\Gamma_\alpha^{(\pm)}(E) \equiv 2\pi\varphi_\alpha(E)|V_\alpha^{(\pm)}(E)|^2$ and $\Gamma_\alpha^{(\pm)'}(E) \equiv 2\pi\varphi_\alpha(E+U)|V_\alpha^{(\pm)}(E+U)|^2$, where $V_\alpha^{(\pm)}(E) = V_\alpha(E) \pm \delta V_\alpha(E)$ ($\delta V_\alpha(E) > 0$), and $\varphi_\alpha(E)$ is the density of states of the electrodes ($\alpha = L, R$). Hereafter, we use $\Gamma_\alpha^{(\pm)}$ s and $\Gamma_\alpha^{(\pm)'}$ s estimated at the Fermi energy μ_α of the electrodes to describe the tunneling rate in the detection process of the qubit states by the two QPCs. This is reasonable from a practical standpoint since many experiments are described using $\Gamma_\alpha^{1,3}$. The values of the corresponding $\Gamma_\alpha^{(\pm)}$ s are determined by the structure of the system such as the distance between the qubits and the QPCs. For example, a $|\downarrow\rangle$ state ($|\uparrow\rangle$ state) in a qubit means the excess charge is localized in the lower (upper) dot, so that the corresponding tunneling rate should be $\Gamma_L^{(-)}$ ($\Gamma_L^{(+)}$). Therefore, two-qubit state $|A\rangle$ would lead to QPC tunneling rates of $(\Gamma_L^{(-)}, \Gamma_R^{(-)})$ or $(\Gamma_L^{(-)'}, \Gamma_R^{(-)'})$, depending on whether or not the island between the QPCs is doubly occupied. Similarly, $|B\rangle$, $|C\rangle$ and $|D\rangle$ states correspond to $(\Gamma_L^{(-)}, \Gamma_R^{(+)})$ [or $(\Gamma_L^{(-)'}, \Gamma_R^{(+)'})$], $(\Gamma_L^{(+)}, \Gamma_R^{(-)})$ [or $(\Gamma_L^{(+)'}, \Gamma_R^{(-)'})$], and $(\Gamma_L^{(+)}, \Gamma_R^{(+)})$ [or $(\Gamma_L^{(+)'}, \Gamma_R^{(+)'})$], res-

spectively.

We construct the equations for the qubit-QPC density matrix elements at zero temperature $T=0$, following the procedure developed by Gurvitz.^{9,11} This method is applicable when the energy level of the inter-QPC island is in between the chemical potentials of the two electrodes. The wave function $|\Psi(t)\rangle$ of the qubit-QPC system can be expanded over the Hilbert space spanned by the two-electron states of the qubits, the island states of the QPC shown in Fig. 1, and all possible electrode states. We choose $|0\rangle$ to refer to the initial ground state of the whole detector system (two electrodes and the inter-QPC island) where the two electrodes are filled with electrons up to μ_L and μ_R , respectively, and the two QPCs and the inter-QPC island are empty of excess electrons. The basis states for the QPC can then be constructed from $|0\rangle$ by moving electrons from the left electrode (with higher chemical potential) to the inter-QPC island and the right electrode. We categorize the detector states by the number of electrons that are transferred from the left to the right electrode (Fig. 1):

$$|\Psi(t)\rangle = |\Psi_0(t)\rangle + |\Psi_1(t)\rangle, \quad (4)$$

where $|\Psi_0(t)\rangle$ is the part of the wave function that no electron tunnels through to the right electrode and $|\Psi_1(t)\rangle$ represents the part of the wave function where one or more electrons are transferred to the right electrode. $|\Psi_0(t)\rangle$ can be expressed as

$$|\Psi_0(t)\rangle = \sum_{z=A,B,C,D} \left\{ b^{(0)a,z}(t) + \sum_{l_s} b_{l_s}^{(0)b,z}(t) d_s^\dagger c_{l_s} + \sum_{l_1 l_2} b_{l_1 l_2 \uparrow \downarrow}^{(0)c,z}(t) d_\uparrow^\dagger d_\downarrow^\dagger c_{l_1 \uparrow} c_{l_2 \downarrow} \right\} |0\rangle |z\rangle, \quad (5)$$

where $b^{(0)a,z}(t)$, $b_{l_s}^{(0)b,z}(t)$ and $b_{l_1 l_2 \uparrow \downarrow}^{(0)c,z}(t)$ are coefficients for the respective states. The superscripts refer to the number of electrons transferred (0 here), the states of the QPC island (as illustrated in Fig. 2), and the four two-qubit basis states. The subscripts refer to the left electrode states from which electrons tunnel into the islands. Thus each of the terms in $|\Psi_0(t)\rangle$ indicates a state with as little as zero but up to 2 electrons moved from the left electrode to the QPC island, while no electron is transferred to the right electrode. $|\Psi_1(t)\rangle$ can be expressed as

$$|\Psi_1(t)\rangle = \sum_{n=1}^{\infty} \sum_{\substack{z=A,\dots,D \\ \beta_1 \dots \beta_n}} \left\{ b_{\beta_1 \dots \beta_n}^{(n)a,z}(t) + \sum_{l_s} b_{l_s \beta_1 \dots \beta_n}^{(n)b,z}(t) d_s^\dagger c_{l_s} + \sum_{l_1 l_2} b_{l_1 l_2 \uparrow \downarrow \beta_1 \dots \beta_n}^{(n)c,z}(t) d_\uparrow^\dagger d_\downarrow^\dagger c_{l_1 \uparrow} c_{l_2 \downarrow} \right\} \otimes \prod_{i=1}^n (c_{l'_i s'_i}^\dagger c_{r'_i s'_i}) |0\rangle |z\rangle, \quad (6)$$

where $\beta_i \equiv (l'_i, r'_i, s'_i)$ represent the left electrode, right electrode, and spin states involved in the transferred electrons. Similar to the expressions of the coefficients for $|\Psi_0(t)\rangle$, here $b_{\beta_1 \dots \beta_n}^{(n)a,z}(t)$, $b_{l_s \beta_1 \dots \beta_n}^{(n)b,z}(t)$ and $b_{l_1 l_2 \uparrow \downarrow \beta_1 \dots \beta_n}^{(n)c,z}(t)$ are coefficients for the states with n electrons transferred to the right electrode, and another 0 to 2 electrons moved from the left electrode to the QPC island. The super-

scripts again refer to the number of transferred electrons (n), the QPC island states, and the qubit basis states.

Substituting this wave function into the Schrödinger equation for the whole qubit-QPC system, $i|\dot{\Psi}(t)\rangle = H|\Psi(t)\rangle$ (having set $\hbar = 1$), we obtain a set of algebraic equations for the coefficients in Eq. (5) and Eq. (6). Assuming zero magnetic field and spin-independent

electron tunneling, the density matrix elements can be defined as

$$\rho_{u_1 u_2}^{z_1 z_2}(t) \equiv \sum_{\beta} \int \frac{dE dE'}{4\pi^2} \tilde{b}_{\beta}^{u_1, z_1}(E) \tilde{b}_{\beta}^{u_2, z_2*}(E) e^{i(E-E')t}, \quad (7)$$

where $\tilde{b}_{\beta}^{u_1, z_1}(E)$ is a Laplace-transformed element of $b_{\beta}^{u_1, z_1}(t)$ after summing over $\beta = \{0, \beta_1, \beta_2, \dots, \beta_n, \dots\}$, the electrode states of transferred electrons as discussed above ('0' corresponds to coefficients in Eq.(5)).

After a lengthy calculation, we obtain 48 equations for the density matrix elements $\rho_u^{z_1 z_2}(t)$, where $u = a, b_{\uparrow}, b_{\downarrow}, c$ indicate quantum states of the inter-QPC island (Fig. 2) as shown in Appendix A.¹² Because we assume that there is no magnetic field, $\rho_{b_{\uparrow}}^{z_1 z_2}(t) = \rho_{b_{\downarrow}}^{z_1 z_2}(t)$.

The readout current is obtained as a time derivative of the number of electrons in the island:^{8,9,11}

$$I(t) = e\Gamma_R [\rho_{b_{\uparrow}}(t) + \rho_{b_{\downarrow}}(t)] + 2e\Gamma'_R \rho_c(t), \quad (8)$$

where ρ_u given by $\rho_u \equiv \rho_u^{AA} + \rho_u^{BB} + \rho_u^{CC} + \rho_u^{DD}$ is the occupation probability of the particular island state u .

As the difference between $\Gamma_{\alpha}^{(+)}$ and $\Gamma_{\alpha}^{(-)}$ increases, the current difference that depends on the difference of qubit states increases as well, while the qubits lose their coherence faster due to the fluctuations in the QPC current, which lead to fluctuations in the qubit energy levels and thus dephasing. We quantify the strength of the measurement by dephasing rates defined as

$$\begin{aligned} \Gamma_d^{\alpha} &\equiv \left(\sqrt{\Gamma_{\alpha}^{(+)}} - \sqrt{\Gamma_{\alpha}^{(-)}} \right)^2, \\ \Gamma_d^{\alpha'} &\equiv \left(\sqrt{\Gamma_{\alpha}^{(+)'}} - \sqrt{\Gamma_{\alpha}^{(-)'}} \right)^2, \end{aligned} \quad (9)$$

where $\alpha = L, R$. These rates are the coefficients of the off-diagonal density-matrix elements of the time-dependent reduced density matrix equations for the qubits. The reduced density matrix elements are

$$\rho^{z_1 z_2} \equiv \rho_a^{z_1 z_2} + \rho_{b_{\uparrow}}^{z_1 z_2} + \rho_{b_{\downarrow}}^{z_1 z_2} + \rho_c^{z_1 z_2}. \quad (10)$$

This definition of dephasing rate is originally introduced by Gurvitz⁹ for the case of a single qubit. The dephasing time is taken as coinciding with the measurement time. Compared with Ref. 9, where there is a single off-diagonal density-matrix element, we cannot define a single dephasing rate because of the complexity of our density-matrix equations.

Current of a QPC in the tunneling regime is very sensitive to the potential variations of the QDs that are set close to the QPC channel.¹³ We thus can choose from a wide range of parameters for our QPCs. Here we use a particular set of representative parameters:

$$\Gamma_A^L = \Gamma_B^L = \Gamma_A^R = \Gamma_C^R = \Gamma^{(-)} = 0.8\Gamma, \quad (11)$$

$$\Gamma_C^L = \Gamma_D^L = \Gamma_B^R = \Gamma_D^R = \Gamma^{(+)} = 1.2\Gamma, \quad (12)$$

which lead to $\Gamma_d^L = \Gamma_d^R (\equiv \Gamma_d) \sim 0.04\Gamma$ for a typical case (Γ is a tunneling rate in the absence of the qubits, so that dephasing rate is more than one order of magnitude smaller, corresponding to a relatively weak measurement). We can regard Γ_d^{-1} as the typical measurement time. Obviously, the qubit dynamics (represented by tunneling rate Ω) would be able to be detected when $\Omega^{-1} < \Gamma_d^{-1}$. Because, in the present setup, the current without qubits saturates in the range of $\sim \Gamma^{-1}$, the time Γ^{-1} would serve as a standard of when measurement started. We can also incorporate the effect of Coulomb interaction by setting $\Gamma_L^{(\pm)'} = 0$ as a limiting case of strong on-site Coulomb blockade ($U \rightarrow \infty$ in Eq. (2) so that no double occupation is possible), while for weak Coulomb interaction on the island we can set $\Gamma_{\alpha}^{(\pm)'} = \Gamma_{\alpha}^{(\pm)}$ at the limit of $U = 0$.

III. QUBIT DYNAMICS WITHOUT DETECTOR

In order to better understand our numerical results and the capability of our QPC detector, it is instructive to first examine the dynamics of both a single qubit and two qubits in the absence of any detector, and discuss how the qubit dynamics is measured by the detector.

We first solve the density matrix equations for a single qubit on the basis of localized single quantum dot states $|\uparrow\rangle$ and $|\downarrow\rangle$:

$$\dot{\rho}_{\uparrow\uparrow} = i\Omega(\rho_{\uparrow\downarrow} - \rho_{\downarrow\uparrow}), \quad (13)$$

$$\dot{\rho}_{\downarrow\downarrow} = i\Omega(\rho_{\downarrow\uparrow} - \rho_{\uparrow\downarrow}), \quad (14)$$

$$\dot{\rho}_{\uparrow\downarrow} = i\Delta\rho_{\uparrow\downarrow} + i\Omega(\rho_{\uparrow\uparrow} - \rho_{\downarrow\downarrow}). \quad (15)$$

For the simple case of $\Delta = 0$ (no voltage bias between the two dots so that qubit dynamics is completely determined by the inter-dot tunnel coupling Ω , which corresponds to the optimal operational point in terms of minimum dephasing as discussed in Ref.¹⁴), and starting from one of the localized states \uparrow -state ($\rho_{\uparrow\uparrow}(t=0) = 1$) or \downarrow -state ($\rho_{\downarrow\downarrow}(t=0) = 1$), we have

$$\rho_{\uparrow\uparrow}(t) = \rho_{\uparrow\uparrow}(0) \cos^2(\Omega t) + \rho_{\downarrow\downarrow}(0) \sin^2(\Omega t), \quad (16)$$

$$\rho_{\downarrow\downarrow}(t) = \rho_{\downarrow\downarrow}(0) \cos^2(\Omega t) + \rho_{\uparrow\uparrow}(0) \sin^2(\Omega t), \quad (17)$$

$$\rho_{\uparrow\downarrow}(t) = \frac{i}{2}(\rho_{\uparrow\uparrow}(0) - \rho_{\downarrow\downarrow}(0)) \sin(2\Omega t). \quad (18)$$

These solutions dictate that the QPC current should essentially be determined by $\rho_{\uparrow\uparrow}(t) - \rho_{\downarrow\downarrow}(t) = [\rho_{\uparrow\uparrow}(0) - \rho_{\downarrow\downarrow}(0)] \cos 2\Omega t$. The oscillatory component of the QPC current should thus be dominated by a 2Ω component (in the case of $\Delta \neq 0$, $2\sqrt{\Omega^2 + \Delta^2/4}$), and the temporal evolution of the current is intimately related to the initial state.

We can also infer information on the two-qubit product states from the detector current in a similar manner because density matrices of the product states are written as $\rho^{AA}(t) = \rho_{\downarrow\downarrow}^L(t)\rho_{\downarrow\downarrow}^R(t)$ and so on. Here we solve the

two-qubit dynamics in the absence of the detector by expanding the density matrix on the basis spanned by the Bell states: $|e_1\rangle=(|\downarrow\downarrow\rangle+|\uparrow\uparrow\rangle)/\sqrt{2}$, $|e_2\rangle=(|\downarrow\downarrow\rangle-|\uparrow\uparrow\rangle)/\sqrt{2}$, $|e_3\rangle=(|\downarrow\uparrow\rangle+|\uparrow\downarrow\rangle)/\sqrt{2}$, and $|e_4\rangle=(|\downarrow\uparrow\rangle-|\uparrow\downarrow\rangle)/\sqrt{2}$ (singlet state). If we assume two identical qubits ($\Omega_L = \Omega_R$ and $\Delta_L = \Delta_R (= \Delta)$), the density matrix equations for the two qubits (without the QPC detector: $\Gamma_d^\alpha = 0$) are written as

$$\begin{cases} \dot{\rho}^{e_4 e_4} = 0 \\ \dot{\rho}^{e_2 e_2} = 2i\Delta(\rho^{e_2 e_1} - \rho^{e_3 e_2}) \\ \dot{\rho}^{e_2 e_4} = -2iJ\rho^{e_2 e_4} - 2i\Delta\rho^{e_1 e_4} \end{cases} \quad (19)$$

$$\begin{cases} \dot{\rho}^{e_1 e_1} = 2i\Omega(\rho^{e_1 e_3} - \rho^{e_3 e_1}) + 2i\Delta(\rho^{e_1 e_2} - \rho^{e_2 e_1}) \\ \dot{\rho}^{e_3 e_3} = -2i\Omega(\rho^{e_1 e_3} - \rho^{e_3 e_1}) \\ \dot{\rho}^{e_1 e_3} = -2i\Omega(\rho^{e_3 e_3} - \rho^{e_1 e_1}) - 2iJ\rho^{e_1 e_3} - 2i\Delta\rho^{e_2 e_3} \end{cases} \quad (20)$$

$$\begin{cases} \dot{\rho}^{e_1 e_2} = -2i\Omega\rho^{e_3 e_2} - 2i\Delta(\rho^{e_1 e_1} - \rho^{e_2 e_2}) \\ \dot{\rho}^{e_2 e_3} = 2i\Omega\rho^{e_2 e_1} - 2iJ\rho^{e_2 e_3} - 2i\Delta\rho^{e_1 e_3} \end{cases} \quad (21)$$

$$\begin{cases} \dot{\rho}^{e_3 e_4} = -2i\Omega\rho^{e_1 e_4} \\ \dot{\rho}^{e_1 e_4} = -2i\Omega\rho^{e_3 e_4} - 2iJ\rho^{e_1 e_4} - 2i\Delta\rho^{e_1 e_4} \end{cases} \quad (22)$$

If $\Delta = 0$, which again corresponds to the optimal operational point, the density matrix equations can be classified into four groups (indicated by the four parentheses above). First of all, Eqs. (19) shows that the probabilities in $|e_2\rangle$ and $|e_4\rangle$ states are time-independent. On the other hand, according to Eq. (20), the probabilities in $|e_1\rangle$ and $|e_3\rangle$ states oscillate as a function of $\{\cos(4\Omega^*t), \sin(4\Omega^*t)\}$ ($\Omega^* \equiv \sqrt{\Omega^2 + J^2/4}$). Meanwhile, Eqs. (21) and (22) indicate that the off-diagonal elements $\{\rho^{e_1 e_2}, \rho^{e_2 e_3}, \rho^{e_3 e_4}, \rho^{e_1 e_4}\}$ contain $\{\cos(2\Omega^*t), \sin(2\Omega^*t)\}$ type of oscillations. Therefore, the occupation probabilities for the product states, $\rho^{AA} = (\rho^{e_1 e_1} + \rho^{e_1 e_2} + \rho^{e_2 e_2} + \rho^{e_2 e_3})/2$, $\rho^{BB} = (\rho^{e_3 e_3} + \rho^{e_3 e_4} + \rho^{e_3 e_4} + \rho^{e_4 e_4})/2$, $\rho^{CC} = (\rho^{e_3 e_3} - \rho^{e_3 e_4} - \rho^{e_3 e_4} + \rho^{e_4 e_4})/2$, and $\rho^{DD} = (\rho^{e_1 e_1} - \rho^{e_1 e_2} - \rho^{e_1 e_2} + \rho^{e_2 e_2})/2$, should all contain $\{\cos(2\Omega^*t), \sin(2\Omega^*t)\}$ oscillations, reconfirming the calculations on single-qubit dynamics at the beginning of this section. Therefore, we should be able to distinguish pure entangled states from pure product states $|A\rangle \sim |D\rangle$ based on whether the detected period of the coherent oscillations is limited to $\{\cos(4\Omega^*t), \sin(4\Omega^*t)\}$ ($|e_1\rangle$ and $|e_3\rangle$) or time-independent ($|e_2\rangle$ and $|e_4\rangle$) in the limit of weak interaction between the qubits and the QPCs. Such behavior is indeed evident in our results as shown in the following section.

IV. NUMERICAL RESULTS OF QPC DETECTION

In Ref.8, we clarified three major issues regarding the capability of the two-island SET by monitoring its time-dependent readout current: (1) the two-qubit product states (eigenstates in the absence of inter-qubit interaction and inter-dot coupling within each qubit) $|A\rangle \sim |D\rangle$ can be distinguished; (2) pure entangled states and pure product states can be distinguished; (3) quantum Zeno

effect is present in a two-qubit system. In the following we show that similar results are obtained for the serially-coupled QPC detector despite its simpler state structure.

Figure 3 shows the time-dependent current at small time $t \sim 0$ in the case of weak Coulomb interaction ($U = 0$) ($\Gamma_\alpha^{(\pm)} = \Gamma_\alpha^{(\pm)}$) assuming that initially the two qubits are in one of the four product states. To calculate the current when the two-qubit initial state is $|A\rangle$, for example, we set $b^{(0)a,A}(0) = 1$ and the other coefficients to zero in the total wave function (Eqs. (5) and (6)), which means that $\rho_{aa}^{AA}(0) = 1$ and other density matrix elements are all zero at $t = 0$. At small t initial state $|A\rangle$ (with both electrons located in the respective lower dots) leads to the strongest suppression of the QPC current, while initial state $|D\rangle$ (with both electrons located in the respective upper dots) the least. States $|B\rangle$ and $|C\rangle$ also produce different QPC currents. The reason is that there is a finite bias between the left and right electrodes, so that current flows only in one direction. Consequently, $|C\rangle$, with the left qubit electron in the upper dot (thus less suppression on current), produces a faster rise in current than $|B\rangle$. Since the product states are not the two-qubit eigenstates, they evolve into superposition states and the corresponding QPC current oscillates. Nevertheless, we can distinguish the four initial product states by the values of the readout current in both $J = 0$ and $J \neq 0$ cases. Hereafter we will focus on the $J = 0$ case. As shown in Fig. 3, the current differences between the four two-qubit states can be detected before the coherent motion of the qubits changes the two-qubit state as $\Omega t < \pi/4$.

One observation we made for charge qubits measured by an SET detector is that the amplitude of the SET current oscillations corresponding to the pure entangled states are smaller than those of the pure product states.⁸ Similar effects are also observed for the QPC detectors here, as indicated in Figs. 4 and IV. A qualitative reason is that the wave functions of the entangled states in the charge qubits extend over both qubits compared to the product states, so that the charge distribution of the entangled states is less effective in influencing the readout current. Quantitatively, for instance, Eq. (19) also dictates that current corresponding to a singlet state should have very weak time dependence. Indeed, Fig. 4 shows strong differences between QPC currents for the singlet state $|e_4\rangle$ and product state $|B\rangle$: the detector current on the singlet state is essentially a smoothly rising function of time, while the current for the product state has an oscillatory component of frequency $\sim 2\Omega$ at $V_g = 0$. We obtained similar current behaviors for other entangled states and product states, where the peaks of the coherent oscillations in the other product states are shifted as inferred from Fig. 3. These features hold as long as the entangled states are close to any of the Bell states, $|e_1\rangle, \sim |e_4\rangle$. Figure IV shows the time-dependent current of the generalized singlet state $\cos\theta|\downarrow\uparrow\rangle + e^{i\varphi}\sin\theta|\uparrow\downarrow\rangle$ in the range of $\varphi = \pi$, $0 \leq \theta \leq \pi/2$. We found that the uniformity of the readout current holds approximately up to

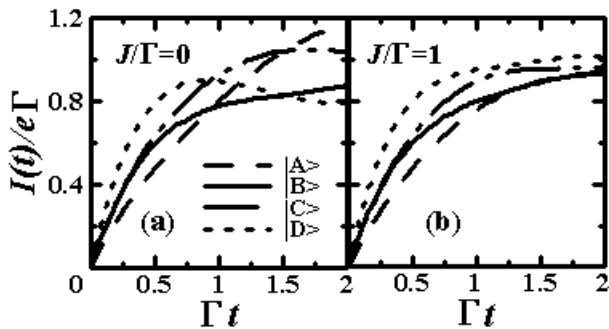


FIG. 3: Time-dependent QPC current $I(t)$ of the $U = 0$ case ($\Gamma_{\alpha}^{(\pm)'} = \Gamma_{\alpha}^{(\pm)}$) starting from four product qubit states $|A\rangle \sim |D\rangle$ at time $t = 0$. $\Omega_L = \Omega_R = 0.75\Gamma$, $\Gamma_d = 0.04\Gamma$. The two panels refer to two different inter-qubit interaction: (a) $J = 0$, (b) $J = \Gamma$. We can distinguish the four product states in both the $J = 0$ case and the $J = \Gamma$ case. This shows that we can distinguish the four two-qubit product states in a range of inter-qubit coupling strength.

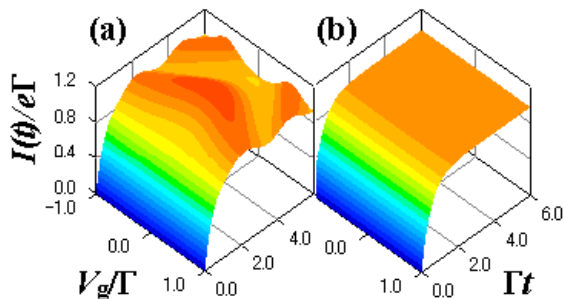


FIG. 4: Time evolution of QPC current $I(t)$ corresponding to the product $|B\rangle$ state (panel (a)) and the entangled singlet state $|e_4\rangle$ (panel (b)) when the qubit gate-bias $V_g (= \Delta_L = \Delta_R)$ changes. The relevant parameters are chosen as $\Omega_L = \Omega_R = 0.75\Gamma$, $J = 0$, $U = 0$ and $\Gamma_d = 0.04\Gamma$. The $I(t)$ for the product state ((a)) explicitly reflects the coherent oscillations of the qubit states, while those for the entangled state are rather uniform.

$|\theta \pm \pi/4| \leq \pi/12$, which is remarkably robust (similar to the case of charge qubits measured by SET detectors⁸). In addition, in Fig. IV, the current for $|C\rangle$ state, another product state, also contains an oscillatory component of frequency $\sim 2\Omega$.

An interesting aspect in studying quantum measurement is to explore the backaction of the measurement apparatus on the qubits. In this context, the quantum Zeno effect refers to the phenomenon that a continuous measurement slows down transitions between qubit quantum states due to the collapse of the qubit wave function into observed states. This phenomenon might be useful in quantum computation because it preserves the results of quantum calculations for a longer period of time.¹⁵ Figure 6 demonstrates the quantum Zeno effect for two qubits measured by the QPC, where the initial state is

chosen to be $|D\rangle$ state ($\rho^{DD}(t=0) = 1$). As the measurement strength increases (Γ_d increases), the oscillations of the density matrix elements of the two qubits are delayed, which is clear evidence of the slowdown described by the Zeno effect.

In general, increasing measurement strength (i.e. the coupling strength between the qubits and the QPCs) leads to faster entanglement between the qubits and the measuring apparatus, so that measurement leads to projection of qubit states into product states. Therefore, stronger measurement strength destroys entangled qubit states more rapidly. This is in contrast to the product states, for which the quantum Zeno effect is observed (Fig. 6).¹⁵ We use the concept of concurrence¹⁶ to quantify two-qubit entanglement and calculate concurrence in the presence of increasing measurement strength. Figure IV shows the effect of measurement on the singlet state, demonstrating that stronger measurement (in the form of larger Γ_d) degrades the entanglement (in terms of concurrence) more rapidly. As seen from Eqs.(13)-(15) and from (19)-(22), product states and entangled states discussed here are generally not two-qubit eigenstates even in the absence of the detector, and thus could evolve into each other through the time-dependent coherent oscillations. Strong detection enhances the mixing of these states and makes it more difficult to infer the qubit states from the detector current. Figures 8 (a) and (b) show the time-dependent currents of $|e_4\rangle$ (singlet state) and $|e_3\rangle$ state as functions of increasing measurement strength. Without the detector, singlet $|e_4\rangle$ state should be time-independent according to Eq.(19), and $|e_3\rangle$ should show 4Ω oscillation according to Eq.(20). Figures 8 (a) and (b) indicate these characteristics in the weak measurement case $\Gamma_d < 0.04\Gamma$, which is also the case that we discussed concerning Fig. 4. In this region, we would be able to distinguish the different behaviors of entangled states and product states. However, as the strength of measurement increases, the detector current starts to acquire other oscillatory components, which means that both states are mixing with other states after $t = 0$. Figure 8 (c) is a time-dependent diagonal matrix element $\rho^{e_4 e_4}$ of the singlet state. This figure also shows that the singlet state mixes with other states as the strength of measurement increases.

In the case of a strong Coulomb interaction so that $\Gamma_L^{(\pm)'} = 0$, we have obtained similar results, except that the magnitude of the average current is reduced by half because the onsite Coulomb interaction closes one transmission channel. This is different from the coupled SET detector we studied before, where current uniformity in finite- U model is more persistent than in the infinite- U model, because the internal degrees of freedom in the two-island SET allow a redistribution of electrons between the islands. Here there is only one island with three island states (unoccupied, singly occupied, and doubly occupied, shown in Fig. 2). The much simpler internal dynamics of these states is insufficient to cause any large change in the QPC current when Coulomb interaction is

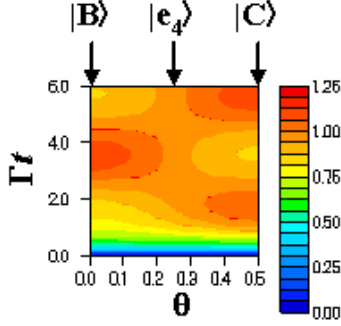


FIG. 5: A contour plot of the time evolution of QPC current for states ranging between $|B\rangle$ state and $|C\rangle$ state through singlet state $|e_4\rangle$ (see text). The current for the “general” singlet state shows uniform characteristics when it is close to the exact singlet state $|e_4\rangle$ as $|\theta \pm \pi/4| \leq \pi/12$. The chosen parameters are similar to what we have before: $\Omega_L = \Omega_R = 0.75\Gamma$, $J = 0$, $V_g = 0$, $U = 0$, and $\Gamma_d = 0.04\Gamma$. In addition, the current for $|C\rangle$ has a oscillatory component of frequency $2\Omega = 1.5$.

accounted for.

V. DISCUSSION

In our study so far we have demonstrated that two-charge-qubit state information can be clearly revealed by the transient current variations in a serially coupled QPC charge detector. An important question is then whether such current evolutions are experimentally observable. In our calculation, Γ , the QPC tunneling rate, is the physical quantity that can be directly connected to experiments. For example, for Γ in the order of 100 MHz, Figs. 3, 4 and 8 show that our scheme requires measurement of a 1 pA current that changes in the nanosecond time scale. This is at the edge of the current technology that allows the measurement of 1 pA current with dynamics in the GHz frequency range with repeated-measurement technique.^{1,3,17,18,19,20}

One issue we have been trying to address in this study is to compare the measurement capability of a QPC detector and an SET detector. In terms of the theoretical descriptions of the qubit-detector interaction, the major difference between the QPC detector studied here and the SET detector in Ref.⁸ is that we model each QPC by a tunnel junction (Ref.⁹), so that the QPC-qubit interaction directly modifies strength of tunneling, while in Ref.⁸, the SET-qubit interaction influences both the SET island state energy and the island-lead tunneling. Despite these differences, our numerical results showed that the current through the coupled QPC exhibits behaviors similar to those of the two-island SET current in many respects, such as in distinguishing the different qubit product states, in distinguishing the Bell-type entangled states from the product states, and in the observation

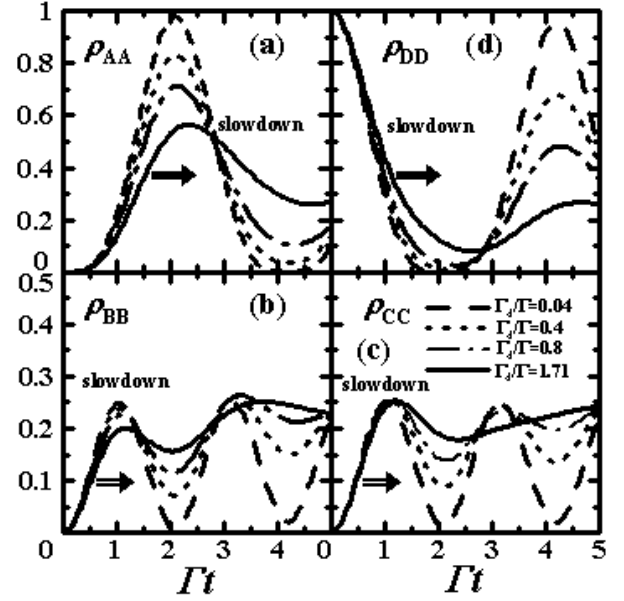


FIG. 6: Time-dependence of $\rho^{AA}(t)$, $\rho^{BB}(t)$, $\rho^{CC}(t)$ and $\rho^{DD}(t)$ for the $U = 0$ case ($\Gamma_\alpha^{(\pm)'} = \Gamma_\alpha^{(\pm)}$), starting from $\rho^{DD}(t=0) = 1$, for different measurement strengths (in terms of Γ_d). Here the intra-qubit tunneling rates are $\Omega_L = \Omega_R = 0.75\Gamma$, and there is no interaction between the qubits: $J = 0$. As measurement strength Γ_d increases, the coherent motions of qubits slow down, which is a clear evidence of the quantum Zeno effect.

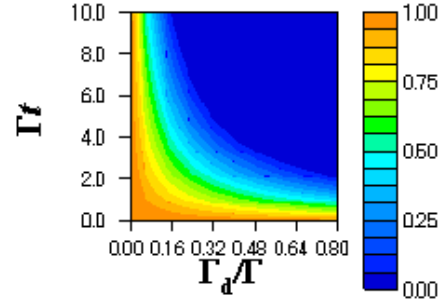


FIG. 7: Time dependent concurrence of a two-qubit state starting from a singlet state $|e_4\rangle$ as a function of the dephasing rate Γ_d in the same parameter region as Fig. IV. At $t = 0$ and $\Gamma_d = 0$, the concurrence takes a value of 1 and rapidly decreases to zero for large dephasing rates.

of quantum Zeno effect for the qubit product states. Stronger differences between QPC and SET detectors do appear when the qubit-detector interaction strength increases. The measurement current of the detector that has a larger number of internal degrees of freedom (the two-island SET) seems to be able to describe more elaborate quantum states of the two qubits. For example, the SET current can clearly distinguish the four product states shown in Ref.8, while with the present QPC de-

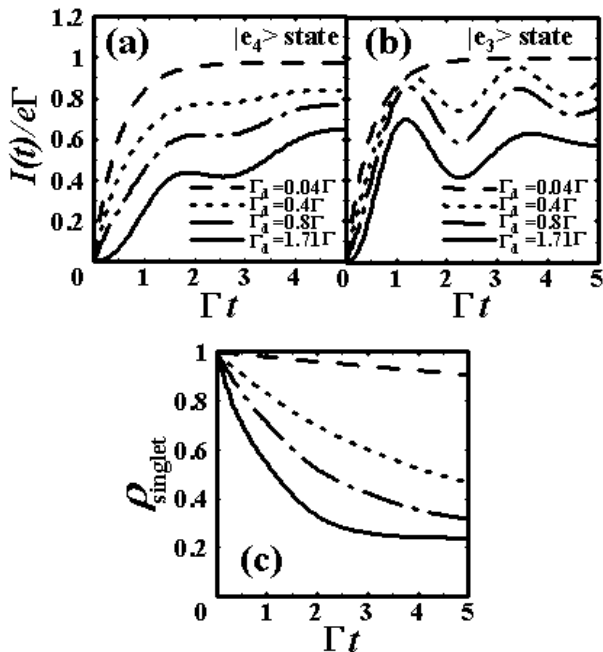


FIG. 8: Time dependent currents for $|e_4\rangle$ (singlet state) (panel (a)) and $|e_3\rangle$ state (panel (b)), and the diagonal density matrix element (panel (c)) for the singlet state, when the dephasing rate Γ_d is changed with $\Delta = 0$. The parameters are the same as those in Fig. IV. At $\Gamma_d < 0.04\Gamma$, Fig.(a) presents the proof of time-independence of the singlet state in Eq.(19), and Fig.(b) shows the proof of the 4Ω oscillation of Eq.(20). Figure (c) shows that the two-qubit state begins to include states other than the singlet states, resulting in the oscillation of the current (panel (a)) when Γ_d becomes large.

tector the current shows a simpler structure and smaller differences for the different qubit states. Qualitatively, the tunneling rate of a QPC is generally larger than that of an SET, which corresponds to shorter dwelling time for the QPC (in the present study the dwelling time for QPCs is effectively taken to be zero). This difference essentially originates from the simpler structure of a QPC compared to an SET.

In the present study we obtained the density-matrix equations under the condition that the voltage bias between the left and right electrodes is sufficiently large such that the left-right symmetry is broken and the transmission of electrons from the right electrode to the left can be neglected. Thus we cannot directly calculate the QPC differential conductance, which would provide more

information for some experiments.¹⁷ This is one of the limitations of the present method. An approach that can properly deal with low bias situations is still in development.

Our configuration of the qubit-QPC coupling scheme can be straightforwardly extended to $N(N > 2)$ -qubit detection. However, it depends strongly on the sensitivity of the current readout circuit such that the 2^N states can be differentiated,⁶ and is thus better suited for only a small number of qubits. In any case, the key objective of the present study is to obtain two-qubit information directly and dynamically, not to invent a general detector for a multi-qubit system, for which other configurations such as a typical one-detector-per-qubit setup are probably more suitable and have to be further studied both experimentally and theoretically.^{18,19,20,21,22} Furthermore, we have considered an ideal measurement process in the present study. In a more realistic situation, imperfections such as gate operation errors,²³ charge fluctuations around the qubit-QPC systems,²⁴ and phonons have to be considered. These imperfections could seriously reduce the sensitivity of a measuring device. Thus more detailed analysis for the coupled multiqubit-detector system needs to be carried out in the future to further clarify these issues.

VI. CONCLUSION

We have solved master equations and described various time-dependent measurement processes of two charge qubits by two serially-coupled QPCs. The current through the QPCs is shown to be an effective means to measure the results of quantum calculations and the presence of entangled states. Two-qubit dynamics is studied analytically and it is found that period of coherent oscillation depends on their initial state. Our results thus show that the serially-coupled QPC can be an effective detector of two-qubit states of a pair of (coupled) charge qubits.

Acknowledgements

We thank N. Fukushima, S. Fujita, M. Ueda, T. Fujisawa and S. Ishizaka for valuable discussion. Also, XH is grateful to ARO and ARDA of the US for support.

APPENDIX A: DERIVATION OF DENSITY MATRIX EQUATIONS

Here we display all the density matrix equations of the qubit-QPC system. The density matrix equations can be classified according to the electronic states of the QPC island (See Fig. 2) and qubit states ($z_1, z_2 = A, B, C, D$, $s = \uparrow, \downarrow$).

$$\frac{d\rho_a^{z_1 z_2}}{dt} = (i[J_{z_2} - J_{z_1}] - [\Gamma_L^{(z_1)} + \Gamma_L^{(z_2)}])\rho_a^{z_1 z_2} - i\Omega_R(\rho_a^{g_r(z_1), z_2} - \rho_a^{z_1, g_r(z_2)}) - i\Omega_L(\rho_a^{g_l(z_1), z_2} - \rho_a^{z_1, g_l(z_2)})$$

$$+ \sqrt{\Gamma_R^{(z_1)} \Gamma_R^{(z_2)}} (\rho_{b\uparrow}^{z_1 z_2} + \rho_{b\downarrow}^{z_1 z_2}), \quad (\text{A1})$$

$$\begin{aligned} \frac{d\rho_{b_s}^{z_1 z_2}}{dt} = & \left(i[J_{z_2} - J_{z_1}] - \frac{\Gamma_L^{(z_1)'} + \Gamma_L^{(z_2)'} + \Gamma_R^{(z_1)} + \Gamma_R^{(z_2)}}{2} \right) \rho_{b_s}^{z_1 z_2} - i\Omega_R (\rho_{b_s}^{g_r(z_1), z_2} - \rho_{b_s}^{z_1, g_r(z_2)}) \\ & - i\Omega_L (\rho_{b_s}^{g_l(z_1), z_2} - \rho_{b_s}^{z_1, g_l(z_2)}) + \sqrt{\Gamma_L^{(z_1)} \Gamma_L^{(z_2)}} \rho_a^{z_1 z_2} + \sqrt{\Gamma_R^{(z_1)'} \Gamma_R^{(z_2)'}} \rho_c^{z_1 z_2}, \end{aligned} \quad (\text{A2})$$

$$\begin{aligned} \frac{d\rho_c^{z_1 z_2}}{dt} = & (i[J_{z_2} - J_{z_1}] - [\Gamma_R^{(z_1)'} + \Gamma_R^{(z_2)'}) \rho_c^{z_1 z_2} - i\Omega_R (\rho_c^{g_r(z_1), z_2} - \rho_c^{z_1, g_r(z_2)}) - i\Omega_L (\rho_c^{g_l(z_1), z_2} - \rho_c^{z_1, g_l(z_2)}) \\ & + \sqrt{\Gamma_L^{(z_1)'} \Gamma_L^{(z_2)'}} (\rho_{b\uparrow}^{z_1 z_2} + \rho_{b\downarrow}^{z_1 z_2}), \end{aligned} \quad (\text{A3})$$

where

$$\begin{aligned} \Gamma_L^{(A)} &= \Gamma_L^{(B)} = \Gamma_L^{(+)} & \Gamma_L^{(C)} &= \Gamma_L^{(D)} = \Gamma_L^{(-)} \\ \Gamma_R^{(A)} &= \Gamma_R^{(C)} = \Gamma_R^{(+)} & \Gamma_R^{(B)} &= \Gamma_R^{(D)} = \Gamma_R^{(-)} \\ \Gamma_L^{(A)'} &= \Gamma_L^{(B)'} = \Gamma_L^{(+)'} & \Gamma_L^{(C)'} &= \Gamma_L^{(D)'} = \Gamma_L^{(-)'} \\ \Gamma_R^{(A)'} &= \Gamma_R^{(C)'} = \Gamma_R^{(+)'} & \Gamma_R^{(B)'} &= \Gamma_R^{(D)'} = \Gamma_R^{(-)'} \end{aligned}$$

and

$$\begin{aligned} J_A &= \Delta_L + \Delta_R + J, & J_B &= \Delta_L - \Delta_R - J, \\ J_C &= -\Delta_L + \Delta_R - J, & J_D &= -\Delta_L - \Delta_R + J. \end{aligned}$$

$g_l(z_i)$ and $g_r(z_i)$ are introduced for the sake of notational convenience and represent relationships between different two-qubit states in the equations for the density matrix elements:

$$\begin{aligned} g_r(A) &= B, g_l(A) = C, & g_r(B) &= A, g_l(B) = D, \\ g_r(C) &= D, g_l(C) = A, & g_r(D) &= C, g_l(D) = B. \end{aligned}$$

-
- ¹ Y. Nakamura, Yu.A. Pashkin, and J.S. Tsai, *Nature* **398**, 786 (1999); Y. Nakamura, Yu.A. Pashkin, T. Yamamoto, and J.S. Tsai, *Phys. Rev. Lett.* **88**, 047901 (2002).
- ² Y. Makhlin, G. Schön, and A. Shnirman, *Rev. Mod. Phys.* **73**, 357 (2001).
- ³ T. Fujisawa, D. G. Austing, Y. Tokura, Y. Hirayama and S. Tarucha, *Nature* **419**, 278 (2002); *Phys. Rev. Lett.* **88**, 236802 (2002); T. Fujisawa, Y. Tokura, and Y. Hirayama, *Phys. Rev. B* **63**, 081304 (2001); T. Hayashi, T. Fujisawa, H. D. Cheong, Y. H. Jeong, and Y. Hirayama *Phys. Rev. Lett.* **91**, 226804 (2003).
- ⁴ W. G. van der Wiel, S. De Franceschi, J. M. Elzerman, T. Fujisawa, S. Tarucha and L. P. Kouwenhoven, *Rev. Mod. Phys.* **75**, 1 (2003); S. Tarucha, D. G. Austing, T. Honda, R. J. van der Hage and L. P. Kouwenhoven, *Phys. Rev. Lett.* **77**, 3613 (1996).
- ⁵ Yu. A. Pashkin, T. Yamamoto, O. Astafiev, Y. Nakamura, D.V. Averin, and J.S. Tsai, *Nature* **421**, 823 (2003); T. Yamamoto, Yu. A. Pashkin, O. Astafiev, Y. Nakamura and J. S. Tsai, *ibid.* **425**, 941 (2003).
- ⁶ T. Tanamoto, *Phys. Rev. A* **64**, 062306 (2001); *ibid.* **61**, 022305 (2000).
- ⁷ A.N. Korotkov, *Phys. Rev. A* **65**, 052304 (2002); R. Ruskov and A. N. Korotkov, *Phys. Rev. B* **66**, 041401 (2002); *ibid.* **67**, 241305 (2003).
- ⁸ T. Tanamoto and X. Hu, *Phys. Rev. B* **69** 115301 (2004).
- ⁹ S. A. Gurvitz, *Phys. Rev. B* **56**, 15215 (1997).
- ¹⁰ I. L. Aleiner, N. S. Wingreen and Y. Meir, *Phys. Rev. Lett.* **79** 3740 (1997).
- ¹¹ S. A. Gurvitz and Ya. S. Prager, *Phys. Rev. B* **53**, 15932 (1996).
- ¹² Compared with the two-island SET detector we considered before,⁸ where we need 352 equations to describe the coupled qubit-detector system, the number of density matrix equations for the QPC detector is significantly reduced.
- ¹³ M. Field, C. G. Smith, M. Pepper, D. A. Ritchie, J. E. F. Frost, G. A. C. Jones, and D. G. Hasko, *Phys. Rev. Lett.* **70**, 1311 (1993).
- ¹⁴ D. Vion, A. Aassime, A. Cottet, P. Joyez, H. Pothier, C. Urbina, D. Esteve, and M.H. Devoret, *Science* **296**, 886 (2002).
- ¹⁵ W. H. Zurek, *Phys. Rev. Lett.* **53**, 391 (1984); L. M. Duan and G. C. Guo, *Phys. Rev. A* **57** 2399 (1998).
- ¹⁶ S. Hill and W.K. Wootters, *Phys. Rev. Lett.* **78** 5022 (1997); W. K. Wootters, *Phys. Rev. Lett.* **80**, 2245 (1998).
- ¹⁷ R. J. Schoelkopf, P. Wahlgren, A. A. Kozhevnikov, P. Delsing, and D. E. Prober, *Science* **280**, 1238 (1998).
- ¹⁸ S. Gardelis, C. G. Smith, J. Cooper, D. A. Ritchie, E. H. Linfield, Y. Jin, and M. Pepper, *Phys. Rev. B* **67**, 073302 (2003); A. W. Rushforth, C. G. Smith, M. D. Godfrey, H. E. Beere, D. A. Ritchie, and M. Pepper, *Phys. Rev. B* **69**, 113309 (2004).
- ¹⁹ P.A. Cain, H. Ahmed, and D.A. Williams, *J. Appl. Phys.* **92**, 346 (2002); *Appl. Phys. Lett.* **78** 3624 (2001).
- ²⁰ R.M. Potok, J. A. Folk, C.M. Marcus, V. Umansky, M. Hanson, and A. C. Gossard *Phys. Rev. Lett.* **91**, 016802 (2003).
- ²¹ J. M. Elzerman, R. Hanson, J. S. Greidanus, L. H. Willems van Beveren, S. De Franceschi, L. M. K. Vandersypen, S. Tarucha and L. P. Kouwenhoven, *Phys. Rev. B* **67**, 161308 (2003); L.-X. Zhang, P. Matagne, and J. P. Leburton, R. Hanson and L. P. Kouwenhoven *Phys. Rev. B* **69**, 245301 (2004).
- ²² L. DiCarlo, H. J. Lynch, A. C. Johnson, L. I. Childress, K. Crockett, C. M. Marcus, M. P. Hanson, A. C. Gossard, *Phys. Rev. Lett.* **92**, 226801 (2004).
- ²³ X. Hu and S. Das Sarma, *Phys. Rev. A* **66**, 012312 (2002).
- ²⁴ T. Itakura and Y. Tokura, *Phys. Rev. B* **67**, 195320 (2003).